

## Analysis of the cone penetration test in layered clay

J. WALKER\* and H.-S. YU†

This paper presents an analysis of the cone penetration test in multi-layered clays using the commercial finite-element code Abaqus/Explicit. The von Mises yield criterion and its associated flow rule are assumed to model the plastic behaviour of elastoplastic undrained clays. An arbitrary Lagrangian–Eulerian scheme and an enhanced hourglass algorithm are adopted to preserve the quality of mesh throughout the numerical simulation. Initially, the behaviour of the penetration resistance is examined in a soil with only two layers. The bottom layer is the weaker of the two and the behaviour of the penetration resistance when the cone approaches the lower layer is studied. The investigation is then extended to study the cone penetration test in a multi-layered clay by sandwiching a weaker clay layer between two stronger clay layers. The thickness of the weaker clay layer is varied and the behaviour of the penetration resistance is studied in relation to the thickness and relative strength of the soil layers. The results are discussed with respect to the soil mechanisms that are present when the cone moves past the relevant layer boundaries so that the position of these boundaries can be determined more accurately.

**KEYWORDS:** clays; in situ testing; numerical modelling

Cette communication présente une analyse de l'essai de pénétrabilité au cône dans des argiles multicouches, en utilisant la norme aux éléments finis commerciale Abaqus/Explicit. On a supposé que le critère de fluage de von Mises, et sa règle de fluage connexe, reflètent le comportement plastique des argiles élastoplastiques non drainées. On adopte un système Lagrangien–Eulerien arbitraire, ainsi qu'un algorithme à sablier renforcé, pour conserver la qualité de la maille tout au long de la simulation numérique. Au départ, le comportement de la résistance à la pénétration est examiné dans un sol à deux couches seulement. La couche inférieure est la plus faible des deux, et on étudie le comportement de la résistance à la pénétration lorsque le cône est proche de la couche inférieure. On poursuit ensuite l'examen pour étudier l'essai de pénétrabilité au cône dans une argile multicouche, en intercalant une couche d'argile plus faible entre deux couches d'argile plus résistante. On varie l'épaisseur de la couche d'argile plus faible, et on étudie le comportement de la résistance à la pénétration relativement à l'épaisseur et à la force relative des couches de sol. On discute des résultats relativement aux mécanismes du sol présents lorsque le cône se déplace au-delà des limites des couches concernées, de façon à déterminer avec plus de précision l'emplacement de ces limites.

### INTRODUCTION

The use of rods to penetrate weak soils and find stiffer strata has been practiced since the end of the 19th century. The test procedure did not develop into a recognisable form until 1934 when it was utilised in ground commonly encountered in the Netherlands (i.e. deltaic deposits) to find the ultimate bearing capacity of piles (Barentsen, 1936). Initial developments utilised a cone with a system of push rods to measure end bearing resistance. This quickly developed into a system which was introduced in Indonesia and used a friction sleeve to measure local skin friction over a short length above the cone (Begemann, 1953). Although introduced in 1948, the electric penetrometer did not come into general use until the late 1960s. The electric penetrometer has an advantage over the mechanical penetrometer because it has the ability to record continuously and automatically end bearing resistance and local skin friction.

Skin friction allows for the determination of the soil type and the cone resistance provides an indication of the soil's strength. Unfortunately, when a cone penetrates through layered soil, the layer boundaries become smeared, making their exact determination difficult. Clearly, this is most significant when penetrating through thin layers of weak soil.

Thus, the objective of this study is to investigate the behaviour of the penetration resistance when a cone passes between soil layers and to understand the soil mechanisms present so that layer boundaries may be accurately identified.

It has been shown that the finite-element (FE) method coupled with an arbitrary Lagrangian–Eulerian (ALE) adaptive mesh is capable of simulating the complete cone penetration process from the soil surface to any depth (Susila & Hryciw, 2003; Walker & Yu, 2006). This allows for the determination of the correct stress field around the penetrometer for any material type under any  $K_0$  condition. The ability of this numerical technique allows the study of the cone penetration test in multi-layered clays.

Earlier work that has been published by the current authors (Walker & Yu, 2006) is used as a basis for this investigation. In this work, an FE analysis together with an adaptive mesh was used to investigate penetration resistance during the cone penetration test in uniform soil. The von Mises failure criterion with its associated flow rule and an elastic-perfectly plastic medium were used to approximate undrained clay. The results were compared with a number of existing solutions including those from Baligh's strain path method (Baligh, 1986), the hybrid strain path method and FE analysis by Teh & Houlsby (1991), the simplified, hybrid strain path and cavity expansion analysis by Yu & Whittle (1999), and the one-step steady-state FE analysis by Yu *et al.* (2000). This comparison is presented in Fig. 1 ( $G$  is the soil's shear modulus and  $s_u$  is the soil's undrained shear strength) where it can be seen that the new adaptive FE results agree well with the large deformation FE analyses of Yu *et al.* (2000) and Teh and Houlsby (1991).

A linear elastic analysis studying the effects of soil

Manuscript received 14 September 2007; revised manuscript accepted 29 January 2010. Published online ahead of print 2 July 2010. Discussion on this paper closes on 1 May 2011, for further details see p. ii.

\* Division of Engineering, University of Nottingham Ningbo, People's Republic of China.

† Department of Civil Engineering, Faculty of Engineering, University of Nottingham, UK.

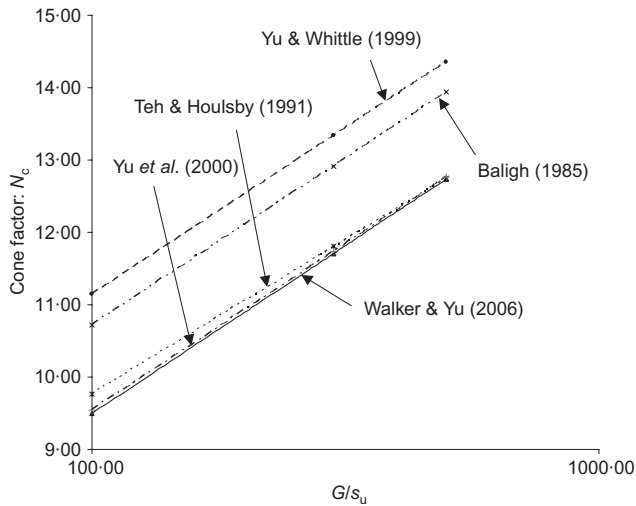


Fig. 1. Comparison of cone factors from various analyses

layering on penetration resistance was carried out by Vreugdenhil *et al.* (1994). The cone was modelled using a body force uniformly distributed over a disc that had the same radius as the cone. The relationship between the body force, load and vertical displacement was analytically approximated and used to investigate the deformation caused by the penetration in an undrained cohesive soil. In this study, Vreugdenhil *et al.* (1994) demonstrated that the cone senses the presence of the approaching layer elastically. Yue & Yin (1999) extended this work using rigorous analytical solutions for the static responses of ring type concentrated body forces and examined soil layering effects in both compressible and incompressible soils.

Van den Berg *et al.* (1996) presented an Eulerian analysis of the cone penetration test in multi-layered soils. The cone was modelled as a fixed boundary and the penetration process was simulated by applying incremental displacements to the material at the bottom of the mesh. The Drucker–Prager and von Mises failure criteria were used to simulate the penetrometer passing from sand into soft clay and vice versa. A minor drawback of this approach is that some numerical diffusion was introduced by the smoothing technique inherent to the convection algorithm.

Meyrhof & Valsangkar (1977) have performed extensive physical model studies of both piles and cone penetrometers in multi-layered soils. The tests included penetration through soft clay or loose sand into dense sand and from dense sand into loose or compact sand. The investigation was extended by performing multi-layered tests with a dense sand layer between two loose sand layers.

However, as outlined above, relatively little analytical or numerical work has been carried out on the cone penetration test in layered soil and, although cone penetration tests are often carried out in layered soils, current geotechnical practice is still based on the cone factors derived from cone penetration analyses in homogeneous soils. The work presented in this paper is one of the earliest numerical studies that aims to investigate the effect of a multi-layer soil on the cone resistance and associated deformation mechanisms. In this respect, it is also relevant to the study of the bearing capacity of driven piles in a multi-layered soil. In particular, the applicability of the single layer analysis is assessed in the light of the parametric studies using different layer thicknesses and stiffness indices.

This paper begins with an analysis of the cone penetration test in a dual-layered undrained clay and this is followed by an analysis of the cone penetration test in a multi-layered undrained clay. The von Mises failure criterion and its

associated flow rule are used to model the soil. The rigidity index of the clay is altered by changing the yield stress while holding the shear modulus constant.

While it may seem unrepresentative of real soil conditions to maintain a constant shear modulus throughout the layers and vary the rigidity index, it must be pointed out that theoretical studies (using cavity expansion theory or strain path analysis) indicate that the key soil property that controls cone resistance for undrained clay is the stiffness index (i.e. shear modulus over undrained shear strength). The stiffness index can be varied in different ways, but they should not affect the numerical solutions. Numerical simulations that altered the rigidity index between layers by varying the shear modulus while holding the shear strength constant proved more difficult to perform with the software used in this study.

## THE DUAL-LAYER MODEL

### Model description

Analyses are performed using the commercial FE package Abaqus/Explicit. The soil is modelled as a weightless undrained clay using the von Mises failure criterion with its associated flow rule, a Poisson ratio of 0.49 and a shear modulus of 1 MPa. A high-quality mesh is maintained throughout each simulation using the ALE adaptive mesh algorithm developed by Van Leer (1977). This algorithm requires the use of first-order elements (i.e. constant strain) hence the analyses use first-order elements and a reduced integration method that is based on the uniform strain method presented by Flanagan & Belytschko (1981) (Abaqus element reference CAX4R). The relative positions of the nodes are adjusted after each loading increment and solution variables are advected between meshes. This prevents over-distortion of the mesh and allows the simulation to run continuously. A refinement of the artificial stiffness method proposed by Flanagan & Belytschko (1981) is used to control hourglassing. This enhanced algorithm is based on the physical hourglass control methods developed by Engelmann & Whirley (1991), Belytschko & Bindeman (1993) and Puso (2000).

The soil is modelled using axisymmetry to reduce the size of the discretised domain. The radius and height of the soil domain are 1.5 m and the cone is modelled using a perfectly smooth rigid surface with the standard cone geometry (apex angle of 60°, cross-sectional area of 1000 mm<sup>2</sup>). A schematic diagram of the model is presented in Fig. 2, where the element sizes are not representative of the actual element sizes used in the model; however, the element grading shown in Fig. 2 is representative of the element grading used in the model. The right-hand boundary is free from initial displacements and stresses.

Figure 2 shows a soil domain comprising two layers. The top layer is 0.3 m deep (8.4 cone diameters) and the bottom layer is 1.2 m deep. In each simulation the cone is pushed a total of 17 cone diameters into the soil. The model is created by attaching two separate soil subdomains together and this is shown in Fig. 3.

Figure 3 shows the constraints and surface interactions that are imposed in the model. Both a frictionless condition and a hard normal contact condition that prevents surface separation exist at the boundary interface (highlighted by arrows). While it is known that the interface between the two layers is not realistically modelled using a perfectly smooth contact condition, the condition is not realistically modelled using a perfectly rough contact condition either. Clearly, further work using different interface conditions will be helpful; however, it is unlikely that the interface condi-

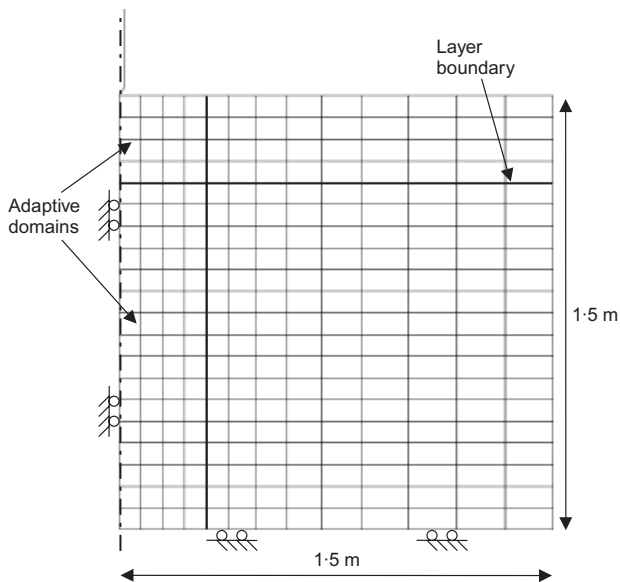


Fig. 2. Dual-layer model

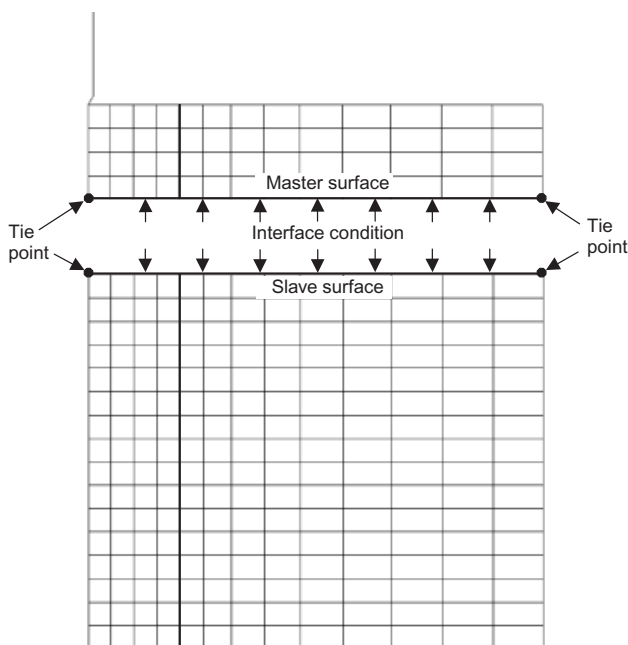


Fig. 3. Boundary constraints and interface conditions

tions will significantly affect the general conclusions drawn from this study.

In Abaqus, the contact algorithm is based on the concept of a master surface and a slave surface. The bodies are first integrated completely independently as if they were not in contact. This uncoupled update indicates which nodes penetrate the master surface during the step (called the slave nodes). The depth of each node's penetration, the mass associated with it and the time increment are used to calculate the force necessary to resist the penetration. If this force had been applied during the increment it would have caused the slave node to lie exactly on the master surface. These forces and the inertial mass of the contacting interfaces are then used to calculate an acceleration correction for the nodes on the slave surface. This is known as a predictor–corrector algorithm.

A hard kinematic condition exists between the contact surfaces (as opposed to a penalty contact condition). This is

a common contact condition where no pressure is transmitted between the surfaces when the nodes are not in contact. When the surfaces are in contact any contact pressure can be transmitted between them. The surfaces separate when the contact pressure reduces to zero.

To allow the adaptive mesh to function properly the two layers do not share common boundary nodes. This condition allows the nodes to slide along the interface but prevents the two surfaces from separating. The tie conditions (i.e. boundary conditions that tie the degrees of freedom of common nodes) are necessary to prevent the top layer from sliding off the bottom layer, to prevent the soil domains splitting along the interface (in spite of the normal contact condition) and to prevent the soil buckling when the cone passes the interface.

Figure 4 shows the soil buckling ahead of the cone face and beginning the creation of a void. Voids like these cause numerical instabilities and are not physically meaningful. Hence, the tie constraints shown in Fig. 3 are imposed on the model.

The total number of elements in the top layer is 10 710, with the majority of those (8010) residing in the top layer's adaptive subdomain. A total of 42 840 elements are used in the bottom layer with the majority of those (22 400) residing in the bottom layer's adaptive subdomain. The simulation is run in three steps with different adaptive domains being active depending on the current stage of the analysis. In step 1, only the top layer's adaptive mesh is active and the cone is pushed to a total depth of 31 cm during 31 s using a time increment of 0.0003 s (the size of the time step controls the size of the displacement increment and mass scaling is used to ensure that the chosen time step is always equal to the critical time step). Although the layer boundary is 30 cm below the soil surface, soil from the layer above is pulled down with the cone when the bottom layer is weaker.

Figures 5(a), 5(b) and 5(c) show the top layer being pushed down ahead of the penetrometer. In this case, the rigidity indices of the top and bottom layers are 100 and 300 respectively. The lines indicate the direction and magnitude of the soil displacement as the penetrometer passes the boundary. When the cone first enters the lower layer (Fig. 5(a)), soil at the cone tip is pushed down ahead of the cone.

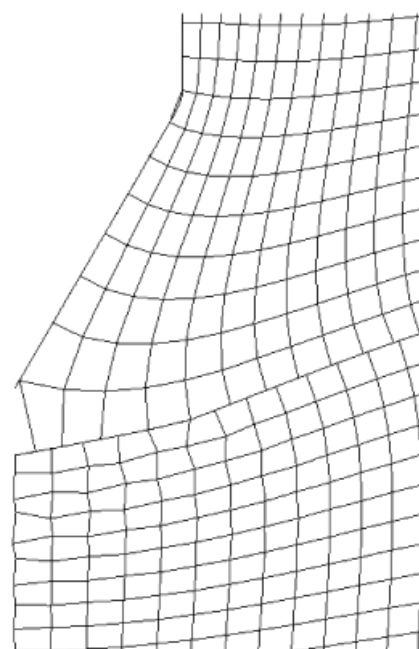


Fig. 4. Element buckling

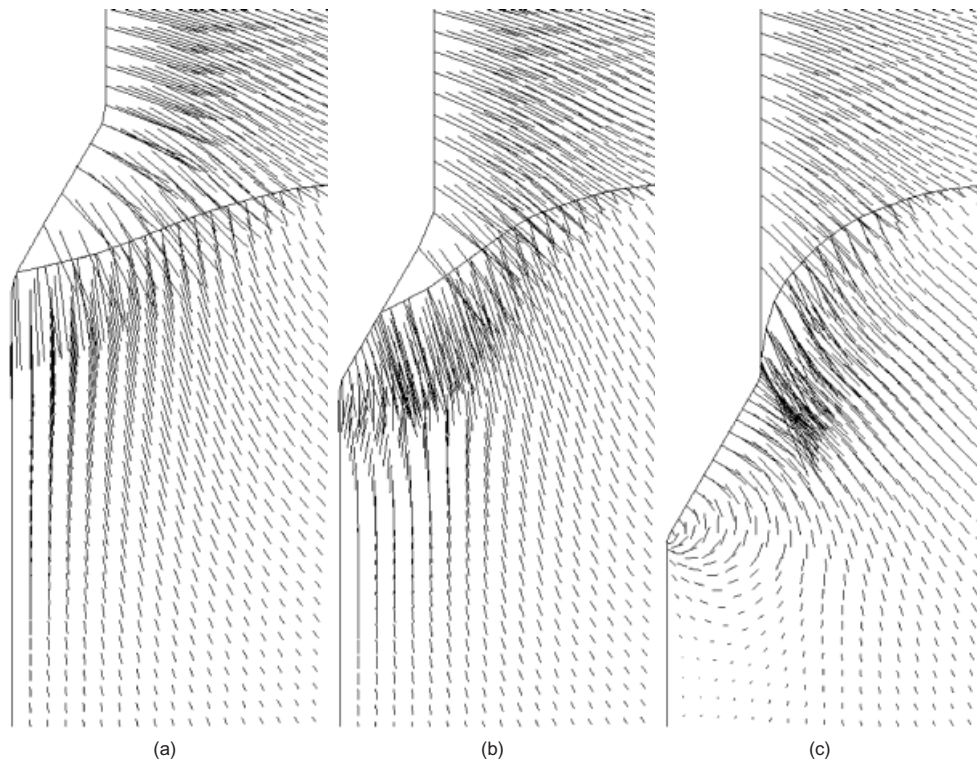


Fig. 5. The displacement field around the cone

This continues until the cone passes into the bottom layer where the displacement at the cone shoulder dominates the solution (Fig. 5(c)).

Step 2 comprises moving the cone just 10 cm further in 10 s at a time increment of  $2.5 \times 10^{-5}$  s. In this step, the adaptive mesh is active in both the top and bottom layers and the adaptive mesh parameters may be altered (depending on the particular analysis) to force the mesh density to increase in areas of high curvature. In Abaqus this is known as curvature refinement and the correct parameters can only be found by trial and error.

Once penetration has progressed past the boundary, the penetrometer is pushed the remaining 19.69 cm in 19.69 s using a time increment of 0.0003 s; the cone penetrates to a total depth of 17 cone diameters (60.69 cm). This is consistent with previous work investigating the numerical modelling of continuous penetration in homogenous undrained clay (see Walker & Yu (2006)). In the final step the adaptive mesh is active in both layers.

#### Testing the model

In order to test the dual-layer model, a simulation is performed with the same material type in both the top and bottom layers. The force on the cone face is provided by Abaqus as a 'field output' and it is calculated by summing the vertical forces at the nodes in contact with the cone face.

Figure 6 shows the force on the penetrometer when it pushes through a von Mises material with a rigidity index of 100 (the solid vertical line is at a depth of 8.4 cone diameters and shows the boundary between the soil layers). Both the dual-layer model and a homogenous model are used and the results are compared. Previous research by the authors (Walker & Yu, 2006) has assessed the ability of the homogenous model to simulate accurately the cone penetration test in various homogenous clays. Interested readers are referred to this paper to see a comparison of the results

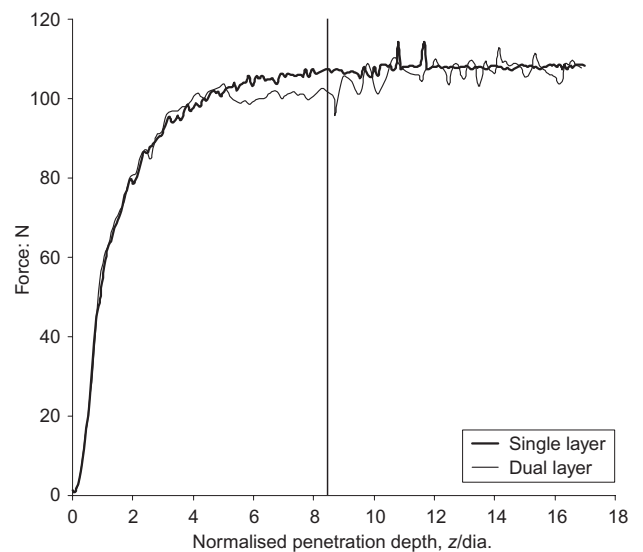


Fig. 6. A comparison between models

generated by the homogenous model with others that can be found in the literature.

It can be seen that the trends are in good agreement up until a penetration depth of 5.04 cone diameters, which is 3.36 cone diameters above the layer boundary. At this point there is a noticeable drop in the vertical force on the penetrometer given by the dual-layer model. This is a result of the interface condition between the top and bottom layers. In the dual-layer model, a frictionless condition exists between the top and bottom layers and clearly this releases constraints on the master surface. A purely rough condition at this interface causes the elements to distort unreasonably as the cone passes. It is known that neither a purely frictionless nor a purely rough condition exists between the two layers and the friction condition at this interface is a subject for further investigation. It can be seen that the two

trends rejoin at a penetration depth of 10.6 cone diameters, after which there is significantly more noise in the output from the dual-layer model.

#### Penetration through varying clays

Now that the differences in the outputs generated by each model have been investigated, the dual-layer model can be used to study the cone penetration test in undrained clays. In each of the following tests, the rigidity index of the top layer is kept at 100 while the rigidity index of the lower layer is increased. The shear modulus is kept constant ( $G = 1$  MPa) throughout the model.

Figure 7 compares the force on the penetrometer when it pushes through a soil with two different rigidity indices, with the force on the penetrometer when it is pushed through a homogenous soil. Both results are obtained using the dual-layer model and the vertical line indicates the layer boundary. The horizontal broken line shows the steady-state penetration resistance in a soil with a rigidity index of 300.

The results first deviate from each other at a depth of 6.25 cone diameters (2.15 cone diameters above the boundary). This is 1.21 cone diameters below the depth at which the cone first senses the boundary (owing to the frictionless condition at the boundary interface). This is significant because it shows that the deviation is due to the difference in the soil strengths. The significant amount of scatter makes it difficult to determine exactly when the cone is no longer affected by the presence of the top layer. A good estimate is approximately two cone diameters below the interface (a total penetration depth of 10.4 cone diameters). This corresponds to the point indicated in Fig. 7 and Fig. 8 shows the position of the cone at this point.

Figure 8 shows the total displacement around the cone when it passes the layer boundary. The cone is modelled using the standard dimensions hence the soil's horizontal displacement next to the shaft is equal to 17.85 mm. There is a linear relationship between vector length and total displacement. It can be seen that at the cone shoulder there is a large vertical displacement directly beneath the layer boundary. At the cone shoulder, the total vertical soil displacement is rarely larger than the total horizontal displacement; however, in this case an exception is seen because the soil in the lower layer is weaker.

Both Figs 6 and 7 show that the cone is unaffected by the top layer as soon as the shoulder of the cone enters

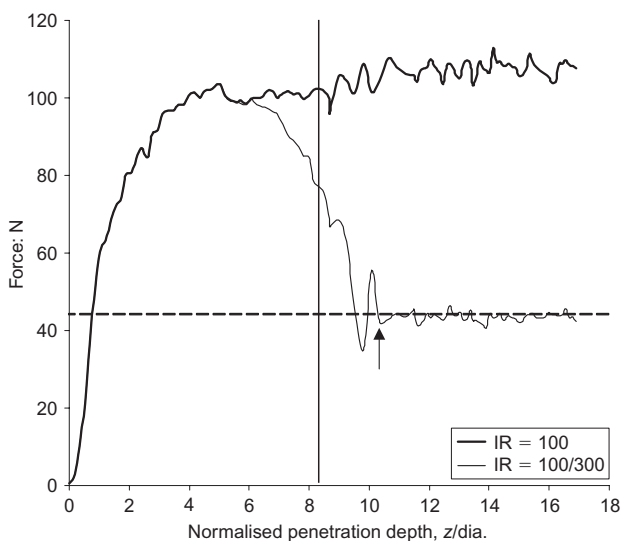


Fig. 7. Penetration resistance in a dual-layered soil (IR, rigidity index)

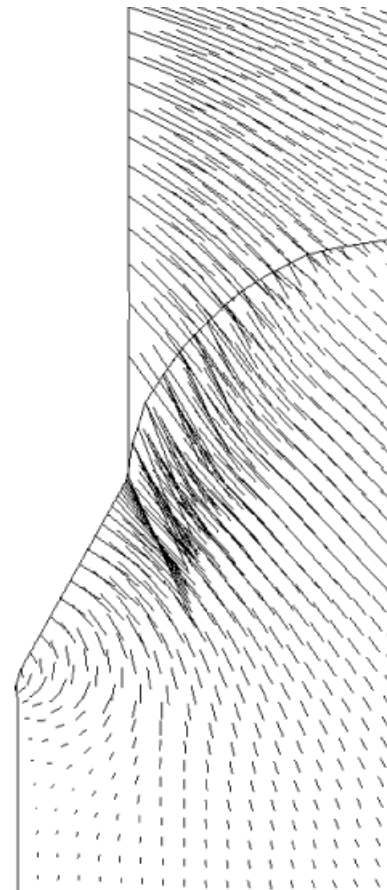


Fig. 8. The displacement field around the cone

the bottom layer. The maximum displacement occurs at the shoulder of the cone and it can be seen that relatively little displacement occurs at the cone tip. At this penetration depth, the soil displacement at the shoulder of the cone dominates the solution and the soil near the cone tip is pushed towards the axis of symmetry.

The results indicate that the upper layer's influence extends two cone diameters below the initial position of the layer boundary. The cone face is 0.87 cone diameters in height meaning that the soil has been pulled down 1.13 cone diameters. Clearly if the roughness of the cone face is increased the upper layer will be pulled down further, extending its influence.

The steady-state penetration resistances in materials with rigidity indices of 100 and 300 are 107.5 N and 43.8 N respectively. The mean of these values is 75.75 N and this is very close to the force on the penetrometer when it passes the initial position of the layer boundary. The influence of the bottom layer on the penetration resistance starts at a depth of 6.25 cone diameters and from this point, the properties of both layers have an effect on the penetration resistance. This continues until the penetrometer completely passes into the bottom layer. This occurs at a depth of 10.4 cone diameters. The mean of 6.25 and 10.4 is 8.325; this is very close to the initial depth of the layer boundary.

It is interesting to extend the study to look at the influence of the soil properties in this situation. The simulation is repeated with the bottom layer having a rigidity index of 500 and the evolution of the penetration resistance is shown in Fig. 9. In this case, the results begin to separate at a depth of 5.8 cone diameters (2.6 cone diameters above the layer boundary). This is at a shallower depth than in the previous case and is expected because the bottom layer is weaker. The cone is not affected by the top layer when the cone has travelled 2.2 cone diameters (10.6 cone diameters

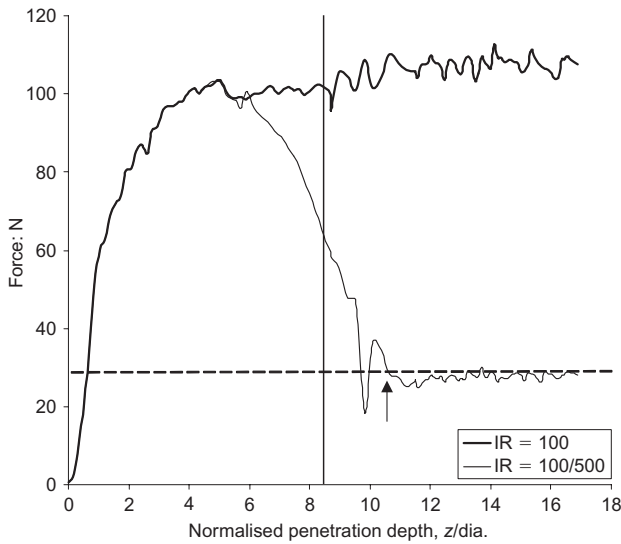


Fig. 9. Penetration resistance in a dual-layered soil

total depth) past the initial position of the boundary. This point is indicated by the arrow in Fig. 9. When compared to the previous case it can be seen that the top layer is pulled down slightly further because of the greater difference in the relative strengths of the materials. The displacement mechanism is the same as that shown in Fig. 8. In other words, the top layer has no influence on the penetration resistance when the shoulder of the cone enters the bottom layer.

The penetration resistances in materials with rigidity indices of 100 and 500 are 107.5 N and 28.2 N respectively. The mean of these values is 67.85 N, which again is very close to penetration resistance when the cone is passing the initial position of the boundary. Likewise, the mean of 5.8 and 10.6 is 8.2; this is also very close to the initial position of the boundary.

The force on the penetrometer when it passes through different materials has been examined. The boundary interface conditions influence the penetration resistance when the cone tip is as much as 3.36 cone diameters above the boundary. The height of influence of the lower, weaker layer depends on the relative strength of the layers. From these results, it appears that the height of influence of the bottom layer on the top layer is marginally greater than the reverse. The cone senses the approaching layer at either 2.15 or 2.6 cone diameters above the boundary (depending on the strength of the bottom layer) and the influence of the upper layer extends for either 2.0 or 2.2 cone diameters into the bottom layer respectively. The force on the penetrometer when the cone passes the initial layer boundary position is close to the mean of the steady-state penetration resistances of the two layers. Finally, it is clear that the top layer has no effect on the penetration resistance once the shoulder of the cone has passed into the bottom layer.

MULTI-LAYERED CLAYS

Model description

The analysis is extended to model undrained clays comprising three layers and the intention is to investigate the effect of layer thickness on the penetration resistance. Ultimately, the accurate location of material boundaries and the correct determination of layer thicknesses are desired.

Figure 10 shows the inclusion of an extra (middle) layer in the model. This layer is prescribed the height  $D$ , which varies in each analysis. The top layer is given a height ( $H$ ) of 0.3 m and  $D$  is varied according to  $H/D = 6, 3, 2$  and 1,

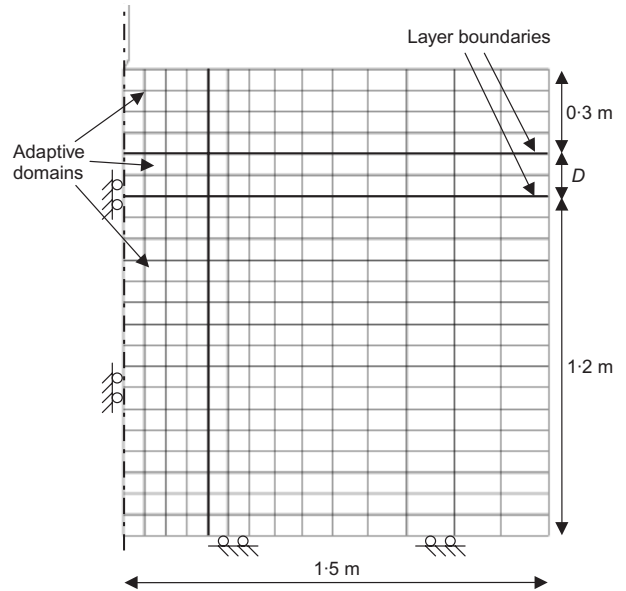


Fig. 10. Multi-layer model

giving layer thicknesses of 5 cm, 10 cm, 15 cm and 30 cm respectively. The interface conditions and constraints are the same as those presented for the dual-layer model and these are shown in Fig. 11.

Once again the interface is frictionless and a hard contact condition that does not allow surface separation exists at each layer boundary. The CAX4R elements with enhanced hourglass control are used throughout the model. The number of elements in the top and bottom layers is the same as the dual-layered model and the number of elements in the middle layer is adjusted depending on its height.

Once again the simulation is run in three steps. The first step lasts 31 s and moves the penetrometer 31 cm into the soil using a time increment of 0.0003 s. The duration of the second step depends on the height of the middle layer. In

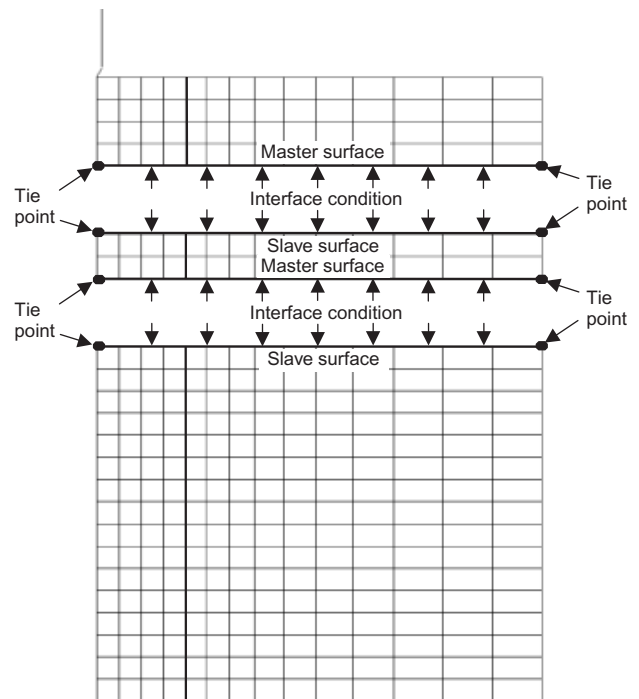


Fig. 11. Boundary constraints and interface conditions

simulations where the middle layer is 3 cm or 5 cm, the second step runs for 10 s and the penetrometer moves 10 cm using a time increment of  $2.5 \times 10^{-5}$  s. This has the effect of slowly moving the cone from the top layer, through the middle layer and far enough into the bottom layer so that the middle layer has no influence on the cone. Likewise, in the models which have a middle layer thickness of 10 cm, 15 cm or 30 cm, the middle step lasts for 15, 20 and 35 s, in which the cone moves 15 cm, 20 cm and 35 cm respectively. The time increment in the middle step is the same in all analyses. The final step involves moving the penetrometer far enough into the bottom layer to be sure that a steady-state penetration resistance has developed.

In the first step, only the top layer's adaptive mesh is active; however, in the second and third steps the adaptive mesh is active in all three layers. Once again, different curvature refinement parameters are used depending on the analysis. Typically, the same parameters are used in steps 1 and 3 (quite often, no curvature refinement is needed in these steps) and the curvature refinement is altered in the second step. These analyses are extremely troublesome and up to seven simulations may be needed to determine the best parameters. If the appropriate parameters are not chosen, then the elements will heavily distort above and below the layer boundary when the cone passes. This will cause the simulation to terminate.

#### Testing the model

Once again, the accuracy of the model output is assessed using the same material type in all three layers. Fig. 12 compares the penetration resistance from both a homogenous model and the multi-layer model using a von Mises material with a rigidity index of 100. In this case the middle layer is 10 cm thick.

The two solid vertical lines in Fig. 12 show the initial positions of the layer boundaries. It can be seen that the curves separate approximately 3.4 cone diameters above the upper soil boundary. This is consistent with the dual-layer model and is caused by the interface conditions. The penetration resistance does not increase again until the cone moves two cone diameters into the bottom layer. This is because the frictionless interface condition between the middle and bottom layers affects the penetration resistance when the cone is in the middle layer.

There is significantly more noise produced by this model

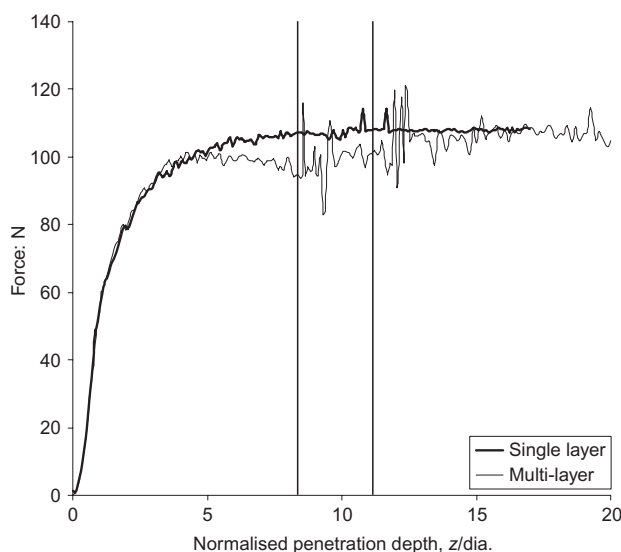


Fig. 12. A comparison between models

and this cannot be eradicated by reducing the time increment. Indeed, some of the largest oscillations occur when the time increment is  $2.5 \times 10^{-5}$  s. It is likely that the noise comes from some elements being over-constrained between the cone, the layer boundary and the tie point. In effect, some locking is exhibited in the elements beneath the boundary when the cone is passing and this is evident by the patchwork effect that can be seen in the element stress contour plots. This is not an element problem and the constraints that are imposed are necessary for the simulation to run continuously.

Now that a benchmark has been set it is possible to alter the strength of the middle layer to investigate the influences of both the layer thickness and the material type on the penetration resistance. The shear modulus is kept constant ( $G = 1$  MPa) and the yield strength is altered to adjust to the rigidity index. The rigidity index of the middle layer is always higher than that of the top and bottom layers and the rigidity index of the top and bottom layers is kept at 100 in the analyses presented here.

#### Penetration through varying clays

Figure 13 presents the penetration resistances as the cone moves through the multi-layered model. The strength of the middle layer is altered to have a rigidity index of either 300 or 500 and the middle layer is 10 cm thick. The vertical lines show the material boundaries and the broken horizontal lines show the steady-state penetration resistances for the respective materials. The behaviour of the penetration resistance in the top layer was investigated earlier when it was concluded that a weaker layer beneath the current layer causes the penetration resistance to fall before the cone reaches the boundary. Correspondingly, the influence of the middle layer increases with the difference in relative strength.

There is a significant amount of noise in the model when the cone enters the middle layer. This is a model problem and was described earlier. When they are well behaved, the results show that the force on the penetrometer in the middle layer is less than the steady-state penetration resistance. This is the result of the frictionless interface condition between the middle and bottom layers. All three simulations show that the penetrometer resistance does not significantly change when the cone is in the middle layer.

When the cone passes into the bottom layer the penetra-

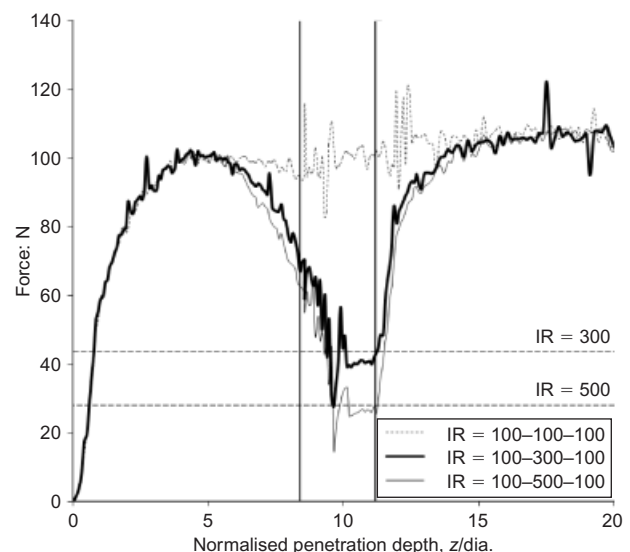


Fig. 13. Penetration resistance in a multi-layered soil

tion resistance rises sharply. The results from the two simulations with weaker middle layers follow each other closely when the cone passes into the bottom layer. Full penetration resistance is developed in the bottom layer at an approximate depth of 15.5 cone diameters which is 4.3 cone diameters beneath the lower material boundary. Meyerhof & Valsangkar (1977) performed a similar cone penetration analysis in a soil comprising a soft clay overlaying a dense sand. In this case, the full penetration resistance was developed approximately 20 cone diameters below the soil boundary. A cone penetration analysis in a homogenous soil comprising the same dense sand showed that steady-state penetration conditions were achieved at a depth of 30 cone diameters. Hence, upon the cone entering the dense sand in the dual-layer test, steady-state conditions were achieved after only two-thirds of the depth required to achieve steady-state conditions in the homogenous soil. Correspondingly, the results presented here show that in the dual-layer model, steady-state conditions are achieved at a little under half of the depth required to achieve steady-state conditions in the relevant homogenous model. This discrepancy can be attributed to the differences in the soil behaviour of sand and clay.

The behaviour of the soil can be understood by observing the penetrometer passing into the bottom layer and this is shown in Fig. 14. In this figure, arrowheads have been included because the direction of the soil displacement at the cone tip is not immediately obvious. The middle layer has a rigidity index of 300 and the bottom layer has a rigidity index of 100.

Figures 14(a), 14(b) and 14(c) show that when the cone tip enters the lower layer the majority of the soil's displacement is horizontal. Upon further penetration the displacement field shows that the lower layer rises in order to accommodate the volume of the cone. Once again, the horizontal displacement around the cone is greatest at the cone shoulder and very small at the cone tip. When the cone moves into the bottom layer, the penetration resistance rises sharply because no soil is pulled down with the cone.

It is clear that the relative yield strengths of the materials have a significant effect on the penetration resistance when the penetrometer passes between them. An interesting area for further research is to investigate the penetration resistance in multi-layered materials which all have the same yield strength but different shear moduli.

*The effect of layer thickness*

The investigation is extended to examine the effect of layer thickness on the penetration resistance. The penetration resistances for four different models are shown in Fig. 15. The models are varied by altering the thickness of the middle layer to 5 cm, 10 cm, 15 cm and 30 cm. The lower boundaries for these layers are shown by the broken vertical lines. The top layer is 30 cm thick in every model and the

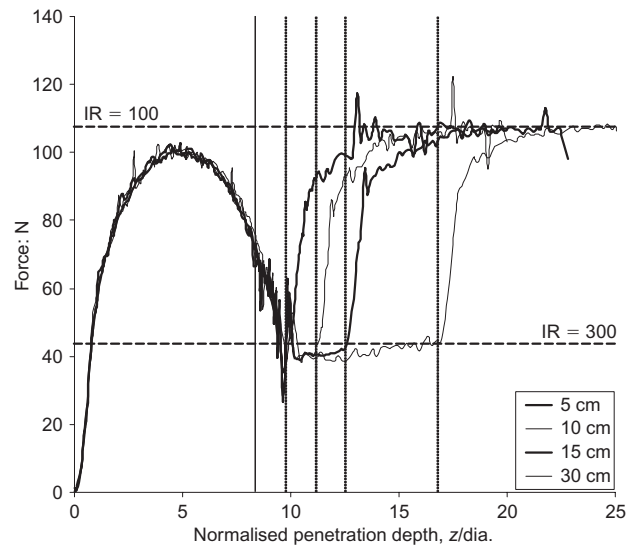


Fig. 15. The effect of layer thickness on penetration resistance

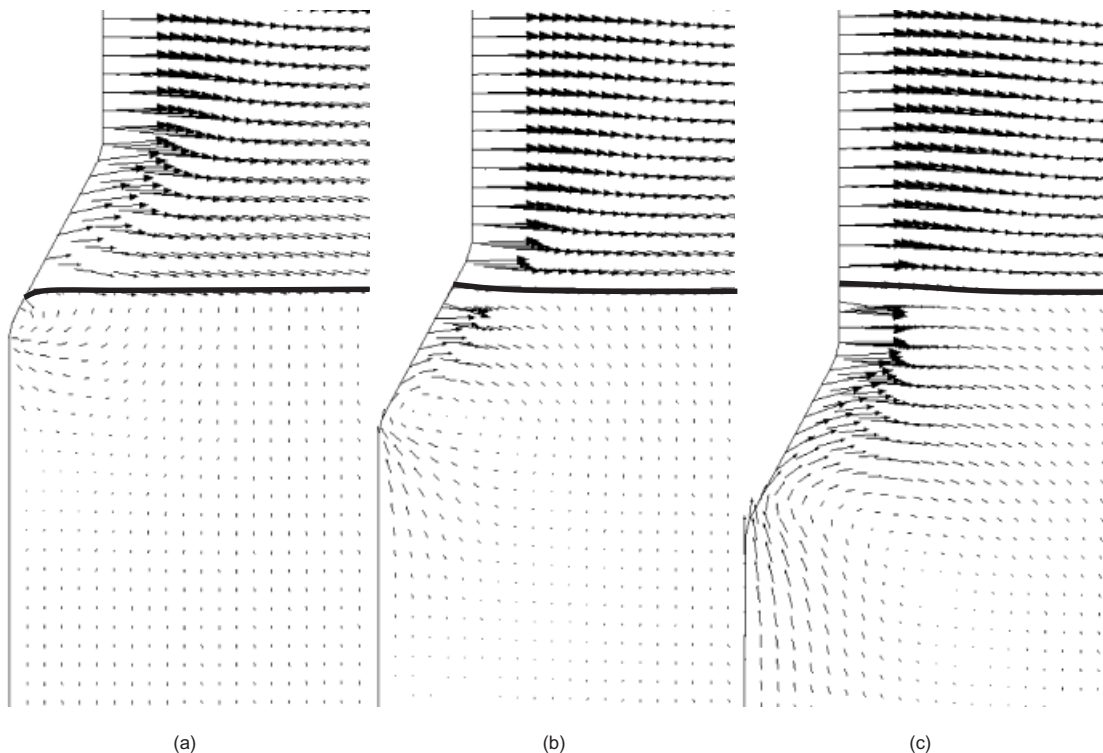


Fig. 14. The displacement field around the cone

position of the boundary between the top and middle layers is shown by the solid vertical line. For each of the results shown, the top and bottom layers have a rigidity index of 100 and the middle layer has a rigidity index of 300.

Figure 15 shows that the layer thickness has no impact on the penetration resistance while the cone is in the top layer. Clearly the penetration resistance is the same in all four cases until the cone enters the middle layer. In each case it can be seen that the penetration resistance rises sharply when the cone enters the stronger, bottom layer and, in this respect, the determination of the lower layer boundary is trivial. In the cases where the middle layer is at least 10 cm thick, the penetration resistance can be seen to rise slightly as the cone approaches the lower boundary. This result is expected because the stronger layer supports the weaker layer above it. In all four cases, the behaviour of the penetration resistance when the cone enters the bottom layer is almost identical.

In the case where the middle layer is 5 cm thick the penetration resistance drops below the steady-state penetration resistance when the cone is in the middle layer. Fig. 7 indicates that the influence of the top layer extends approximately two cone diameters (7.14 cm) into the underlying weaker layer. Hence, in the 5 cm model it is likely that numerical oscillations cause this drop in the penetration resistance. The phenomenon is investigated using a model with a middle layer thickness of 3 cm and the result is shown in Fig. 16.

In Fig. 16 the two solid vertical lines represent the layer boundaries and the horizontal broken lines indicate the relevant steady state penetration resistances. When the cone approaches the upper soil boundary, the penetration resistance reduces and continues to reduce until the cone tip reaches the bottom boundary. If the point that is indicated is considered erroneous, then the penetration resistance remains constant until the cone shoulder passes into the bottom layer and at this point the penetration resistance rises sharply. The displacement mechanism for this process is shown in Fig. 17.

Figures 17(a), 17(b) and 17(c) show the cone passing through a thin layer of material which is just 3 cm thick. The displacement field shows that the soil is pushed down ahead of the cone when the cone approaches the middle layer. Clearly, the middle layer reduces in height as the cone

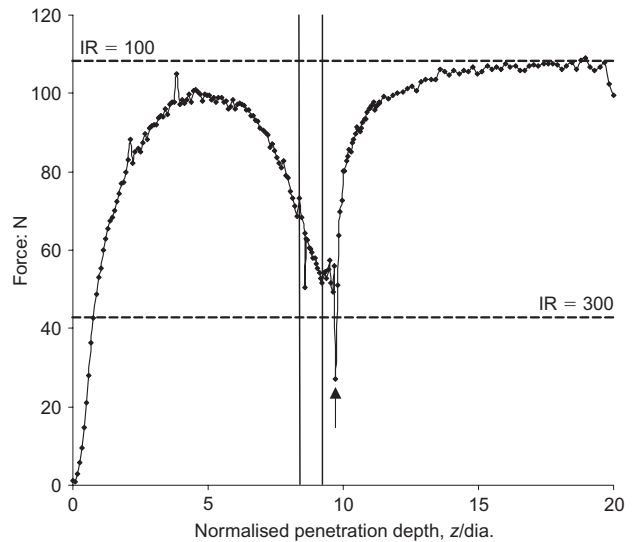


Fig. 16. Penetration resistance through a very thin layer

pushes past it and the cone is never fully supported by the weaker material in the middle layer. Thus, the penetration resistance will not reduce to the steady-state penetration resistance of the middle layer.

It can be concluded that when the middle layer is less than two cone diameters in height, the penetration resistance will continuously fall throughout the middle layer until the cone tip reaches the bottom layer. At this point, the penetration resistance remains constant until the shoulder of the cone passes the lower boundary, when the penetration resistance rapidly increases with depth until steady-state conditions are achieved. In this case, the penetration resistance is dependent on the layer thickness and the rigidity indices of all three layers.

The investigation is extended further by substituting the middle layer for a von Mises material with a rigidity index of 500 and repeating the simulations. The results are presented in Fig. 18.

Once again, the vertical lines show the boundaries between the soil layers and the broken horizontal lines show the steady-state penetration resistances for the relevant mate-

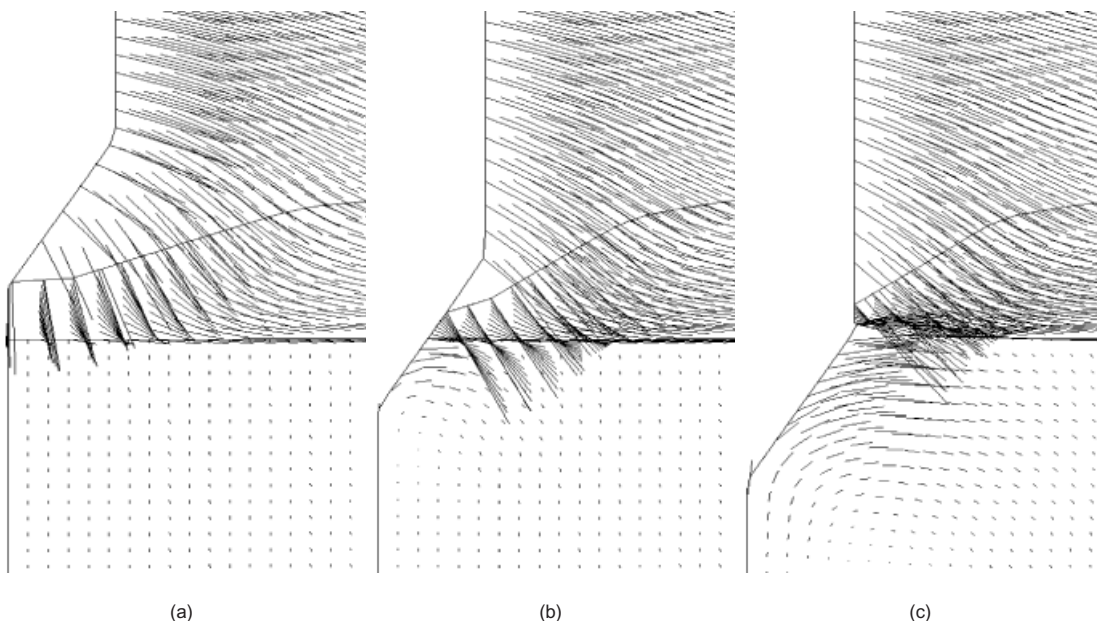


Fig. 17. The displacement field around the cone

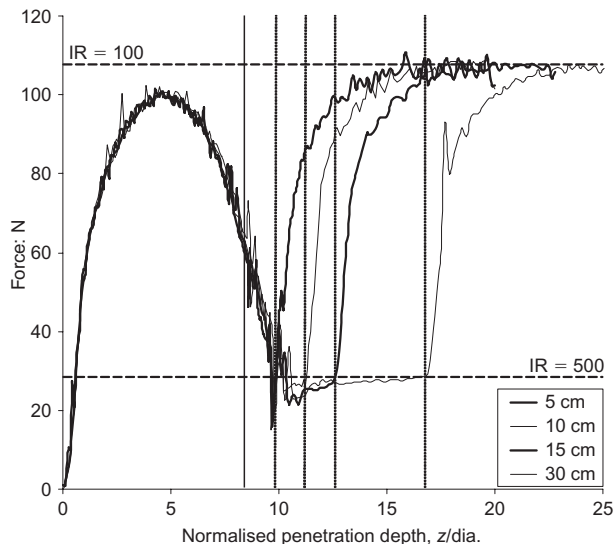


Fig. 18. The effect of layer thickness on penetration resistance

rials. There is little separation of the results in the top layer and the first divergence occurs in the middle layer. The penetrometer is able to sense the stronger clay in the bottom layer when the cone is in the middle layer and this causes the penetration resistances to rise gradually. The penetration resistance increases sharply when the cone enters the bottom layer. Once the cone is in the bottom layer, the behaviour of the penetration resistance is almost identical in each case. The results show no anomalies when compared with Fig. 15.

It can be concluded that the middle layer thickness has no effect on the penetration resistance when the penetrometer is in the top layer. The penetration resistance will only drop to the steady-state penetration resistance for that particular material if the height of the middle layer is greater than two cone diameters. In these cases, the presence of the stronger, bottom layer will cause the penetration resistance to rise slightly when the cone is in the middle layer. This will continue until the cone enters the bottom layer, where the penetration resistance will sharply rise until steady-state conditions are achieved.

## CONCLUSION

The cone penetration test in multi-layered clays has been investigated using an explicit FE method with an adaptive mesh. The dependence of the penetration resistance on layer thickness and soil properties has been investigated. It has been found that when the cone passes from a stronger layer to a weaker layer, the penetration resistance is significantly influenced either side of the layer boundary. In contrast, when the penetrometer passes from a weak layer to a stronger layer, the change in the penetration resistance is abrupt and the position of the layer boundary can be accurately determined. This multi-layered analysis has shown that layer thickness is not particularly important unless the layer becomes too thin to support the cone fully when the cone passes through it. In these cases, the cone penetration

test will not accurately predict the position of the layer boundaries or the middle layer's soil strength.

## ACKNOWLEDGEMENT

The authors would like to thank Dr Ed Ellis of the Nottingham Centre for Geomechanics for his valuable assistance during the course of this work.

## REFERENCES

- Baligh, M. M. (1985). Strain path method. *J. Geotech. Engng. ASCE* **111**, No. 9, 1108–1136.
- Baligh, M. M. (1986). Undrained deep penetration. I: shear stresses. *Géotechnique* **36**, No. 4, 471–485, doi: 10.1680/geot.1986.36.4.471.
- Barentsen, P. (1936). Short description of a field method with cone shaped sounding apparatus. *Proc. 1st Int. Conf. Soil Mech. Found. Engng, Massachusetts* **1**, 7–10.
- Begemann, H. K. S. (1953). Improved method of determining resistance to adhesion by sounding through a loose sleeve placed behind the cone. *Proc. 3rd Int. Conf. Soil Mech. Found. Engng, Zurich* **1**, 213–217.
- Belytschko, T. & Bindeman, L. P. (1993). Assumed strain stabilization of the eight node hexahedral element. *Comput. Methods Appl. Mech. Engng* **105**, No. 2, 225–260.
- Engelmann, B. E. & Whirley, R. G. (1991). A new explicit shell element formulation for impact analysis. In *Computational aspects of contact, impact and penetration* (eds R. F. Kulak and L. E. Schwer), chapter 3. Lausanne, Switzerland: Elsevier International.
- Flanagan, D. P. & Belytschko, T. (1981). A uniform strain hexahedron and quadrilateral with orthogonal hourglass control. *Int. J. Numer. Methods Engng* **17**, No. 5, 679–706.
- Meyerhof, G. G. & Valsangkar, A. J. (1977). Bearing capacity of piles in layered soils. *Proc. 9th Int. Conf. Soil Mech. Found. Engng, Japan* **1**, 645–650.
- Puso, M. A. (2000). A highly efficient enhanced strain physically stabilized hexahedral element. *Int. J. Numer. Methods Engng* **49**, No. 8, 1029–1064.
- Susila, E. & Hryciw, R. (2003). Large displacement FEM modelling of the cone penetration test in normally consolidated sand. *Int. J. Numer. Analyt. Methods Geomech.* **27**, No. 7, 585–602.
- Teh, C. I. & Houlsby, G. T. (1991). An analytical study of the cone penetration test in clay. *Géotechnique* **41**, No. 1, 17–34, doi: 10.1680/geot.1991.41.1.17.
- Van den Berg, P., De Borst, R. & Huetink, H. (1996). An Eulerian finite element model for penetration in layered soil. *Int. J. Numer. Analyt. Methods Geomech.* **22**, No. 10, 791–818.
- Van Leer, B. (1977). Towards the ultimate conservative difference scheme III. Upstream-centred finite-difference schemes for ideal compressible flow. *J. Comput. Physics* **23**, No. 3, 263–275.
- Vreugdenhil, R., Davis, R. & Berrill, J. (1994). Interpretation of cone penetration results in multi-layered soils. *Int. J. Numer. Analyt. Methods Geomech.* **18**, No. 9, 585–599.
- Walker, J. & Yu, H. S. (2006). Adaptive finite element analysis of cone penetration in clay. *Acta Geotechnica* **1**, No. 1, 43–58.
- Yu, H. S. & Whittle, A. J. (1999). Combining strain path analysis and cavity expansion theory to estimate cone resistance in clay. Unpublished notes.
- Yu, H. S., Herrmann, L. R. & Boulanger, R. W. (2000). Analysis of steady cone penetration in clay. *J. Geotech. Geoenviron. Engng. ASCE* **126**, No. 7, 594–605.
- Yue, Z. Q. & Yin, J. H. (1999). Layered elastic model for analysis of cone penetration testing. *Int. J. Numer. Analyt. Methods Geomech.* **23**, No. 8, 829–843.